

## PHOTOEVAPORATION OF A BINARY PROPLYD SYSTEM

M. J. Vasconcelos,<sup>1</sup> A. H. Cerqueira,<sup>1</sup> A. C. Raga,<sup>2</sup> and R. R. Amorim<sup>3</sup>

*Received 2009 September 21; accepted 2009 November 16*

### RESUMEN

Presentamos simulaciones 3D de la fotoevaporación de un sistema binario de discos de acreción dentro de una región fotoionizada. Las simulaciones consideran la radiación ultravioleta lejana y extrema (FUV y EUV) de una estrella. Estudiamos dos casos: modelos dominados por la radiación FUV y por la EUV. Los modelos dominados por la radiación FUV muestran una cáscara inter-proplyd que está bien definida tanto en mapas de densidad como de emisión  $H\alpha$  cuando la separación de la binaria es relativamente grande ( $\sim 2000$  AU). Para separaciones menores ( $\simeq 200$  AU), no se desarrolla una cáscara inter-proplyd. Mostramos que un modelo EUV con una elección de parámetros adecuada tiene una cáscara inter-proplyd con una emisión de  $H\alpha$  incrementada respecto a la emisión de los frentes de ionización, en mejor acuerdo con las observaciones del proplyd binario LV1.

### ABSTRACT

We present 3D numerical simulations of photo-evaporation of a binary accretion disk system inside an H II region. The simulations take into account far- and extreme-ultraviolet (FUV and EUV) radiation from a stellar source. We study both FUV dominated and EUV dominated models. FUV dominated models show a well defined interproplyd shell in both  $H\alpha$  emission and density maps, when the separation of the binary system is relatively large ( $\sim 2000$  AU). For smaller separations ( $\simeq 200$  AU), the interproplyd shell no longer develops. We show that an EUV model with a suitable choice of parameters increases the  $H\alpha$  emission of the interproplyd shell relative to the emission of the ionization fronts, in better agreement with the observations of the binary proplyd LV1.

*Key Words:* H II regions — stars: circumstellar matter — stars: mass loss — stars: pre-main sequence

### 1. INTRODUCTION

Observations of the star formation region around the Trapezium cluster in M42 (the Orion nebula) reveal several circumstellar disks in silhouette, and also compact emission regions which correspond to material which is being photoevaporated from young stellar object (YSO) systems. These so-called proplyds show a wealth of observational features, like emission line cusps, stationary shocks, microjets, tails, shadows, etc. (O'Dell & Wen 1994; O'Dell & Wong 1996; Smith et al. 2005).

The basic process that explains at least part of the observed proplyd features is the interaction between the UV flux of an external high-mass star with an accretion disk around a low mass YSO. Essentially, the incidence of the ultraviolet radiation field at the disk surface generates a photo-evaporated wind, which interacts with both the photon flux and the wind (or the expanding H II region) that come from the OB association. Previous analytical and numerical models were able to reproduce some of the main features observed in proplyds, like the presence of a crescent in front of the proplyd, the tear-drop shaped tail, the emission at the stationary shock front and the production of microjets (Johnstone, Hollenbach, & Bally 1998; Störzer & Hollenbach 1999; Richling & Yorke 2000; García-Arredondo, Henney, & Arthur 2001).

<sup>1</sup>LATO-DCET, Universidade Estadual de Santa Cruz, Ilhéus, Bahia, Brazil.

<sup>2</sup>Instituto de Ciencias Nucleares, Universidad Nacional Autónoma de México, Mexico.

<sup>3</sup>Instituto Nacional de Pesquisas Espaciais, São José dos Campos, São Paulo, Brazil.

In this paper, we present the first report of a fully three-dimensional numerical simulation of proplyds, in which both the FUV and the EUV radiation fields are included. We present the results obtained for an interesting problem: a pair of proplyds forming a binary system, like the LV1 proplyd (168–326) in Orion. This problem was first addressed by Graham et al. (2002) who analyzed optical and radio observations of LV1 and then suggested that besides the individual ionization fronts observed for each single proplyd, there was an emission region, strong in  $H\alpha$  and [O III] which results from the interaction between the two photoevaporated flows. Later on, Henney (2002) presented an analytical model for this interaction and the formation of the shock structure resulting from the interaction, called interproplyd shell. Here we present 3D simulations from which we are able to compute the  $H\alpha$  emission of the interproplyd shell, where the two mildly supersonic photoevaporated winds collide.

Our simulations are similar to the work of Lim & Mellema (2003), who studied the 3D interaction between two spherical clumps and an impinging ionizing radiation field. Our simulations have a similar resolution to the ones presented by these authors. However, our models have two main differences with respect to the previous work: we consider the photoevaporation of flattened, disk-like structures (as opposed to the spherical clumps considered by Lim & Mellema 2003), and we include the photodissociating, FUV radiation field (only the ionizing radiation was considered by Lim & Mellema 2003). Also, Lim & Mellema (2003) restricted their models to the case in which one of the two neutral clumps shields the other clump from the impinging ionizing radiation. In the present paper we consider the case of two “side by side” disks, both of which receive the unshielded ionizing/dissociating radiation field. This problem is relevant for the geometry found in the LV 1 proplyd (see Henney 2002). In addition, we should emphasize that we have neglected the treatment of the diffuse radiation field, which is known to play an important role in the non-illuminated side of proplyds (see Richling & Yorke 2000). We plan to present three-dimensional calculations of proplyds, taking properly into account the diffuse radiation field in a future paper.

The paper is organized as follows. In § 2 we present the numerical setup and the physical parameters used in the simulation. In § 3 we present our results and in § 4, the conclusions.

## 2. THE NUMERICAL METHOD AND THE SIMULATED MODELS

The 3D numerical simulations have been carried out with the Yguazú-a code (Raga, Navarro-González, & Villagrán-Muñiz 2000) using a 5-level binary adaptive grid. The Yguazú-a code integrates the gas-dynamic equations employing the *flux vector splitting* scheme of van Leer (1982) together with a system of rate equations for atomic/ionic species. In our simulations, we solve them for H I, H II, C I and C II. This code, that can also incorporate other chemical species, has been extensively employed for simulating astrophysical flows (see Cerqueira et al. 2006b, and references therein).

In the present work, we treat the photo-dissociated region (hereafter PDR) as a carbon ionization region, following Richling & Yorke (2000). Instead of solving an energy equation, we have imposed a temperature law of the form:

$$T = (T_1 - T_2) \times x_{\text{HII}} + T_2 \times x_{\text{CII}} + T_3 \times (1 - x_{\text{CII}}), \quad (1)$$

where  $T_1 = 10\,000$  K is the characteristic temperature of an H II region,  $T_2 = 1\,000$  K, is a typical PDR temperature,  $T_3 = 10$  K is the temperature of the neutral gas,  $x_{\text{HII}}$  is the hydrogen ionization fraction, and  $x_{\text{CII}}$  is the carbon ionization fraction. This prescription is justified if the thermal equilibrium time scale is much smaller than the dynamical time scale (Lefloch & Lazareff 1994), which is the case here for both the ionized and the neutral gas. It is clear from equation (1) that we may have a continuous interval in temperature, ranging from 10 K to  $10^4$  K. It follows from this equation that the temperature of the PDR is limited by (but not fixed to)  $10^3$  K. We want to anticipate that, as the system evolves, we found that the temperatures inside the PDR range from 750 K to 950 K, according to the ionization fraction of C II. Also, it is worthwhile to note that considerations on the FUV fluxes that are typically found in the Orion Nebula lead to the conclusion that the PDR of a proplyd must be heated to a temperature of the order of 1 000 K (Tielens & Hollenbach 1985; Johnstone et al. 1998), at the distance of LV1 (from  $\theta^1$  Ori C). We have carried out numerical experiments with different values of  $T_2$  in equation (1). We chose  $T_2 = 800$  K and  $T_2 = 400$  K, which are too low when compared with those expected in PDRs in Orion nebula, as we mentioned before. The differences will be discussed in the conclusions.

Together with the gasdynamic equations, the code integrates radiative transfer equations for photons at the Lyman limits of H I and C I. The trans-

TABLE 1  
SIMULATED MODELS

Model	$D^a$ (pc)	$R_D$ (AU)	$D^b$ (AU)	$S_{\text{EUV}}$ ( $\times 10^{48} \text{ s}^{-1}$ )	$S_{\text{FUV}}$ ( $\times 10^{49} \text{ s}^{-1}$ )
M0	0.1	104/130	2000	7.2	0
M1	0.1	104/130	2000	7.2	1.78
M2	0.1	30/30	214	7.2	1.78
M3	0.01	30/30	214	7.2	1.78

<sup>a</sup>Distance from the source to the center of mass of the proplyd system.

<sup>b</sup>Distance between the center of each proplyd.

fer from a point source (i.e., the central star of the photoionized region) to all of the cells of the computational grid is done with the “short characteristics” method, in which the intensity at a given cell is computed by propagating the intensities at nearby grid points (lying in between the cell and the photon source), with the appropriate extinction. This method has been described in detail, e.g., by Raga et al. (1997) and Mellema et al. (1998). The particular implementation of the short characteristics method which we are using in the present simulations is described by Cerqueira et al. (2006a). The intensity at the HI and CI Lyman limits are then used to calculate the photoionization rates of HI and CI, respectively.

The computational box has dimensions of  $(13.4, 6.7, 6.7) \times 10^3$  AU in models M0 and M1 (see Table 1) and  $(3.3, 1.6, 1.6) \times 10^3$  AU in models M2 and M3, with the longer dimension along the direction of propagation of the ionizing/dissociating radiative field ( $x$ -direction). We use a 5-level, binary adaptive grid with a maximum resolution of 26.0 AU (along the three axes) for models M0 and M1, and of 6.5 AU for models M2 and M3. With this combination of domain sizes and resolutions, all of the simulations have  $512 \times 256 \times 256$  points at the finer grid refinement level.

An external star generates the fluxes of FUV and EUV radiation. We modeled it as a point source located outside the computational domain (Cerqueira et al. 2006a). The source lies at a distance of  $20.6 \times 10^3$  AU (models M0, M1 and M2) and  $2.1 \times 10^3$  AU (model M3) from the proplyd binary system centroid. We choose  $S_{\text{EUV}} = 7.2 \times 10^{48} \text{ s}^{-1}$  and  $S_{\text{FUV}} = 1.78 \times 10^{49} \text{ s}^{-1}$ . These values were taken from Richling & Yorke (2000), who calculated them based on the assumptions that  $\theta^1$  Ori C radiates as a blackbody with  $T_{\text{eff}} = 38500$  K and has a luminosity of  $1.47 \times 10^5 L_{\odot}$ , which is representative of an O6-7 spectral type star.

Each proplyd is modeled as a disk, with a constant thickness  $H = 32.8$  AU for models M0 and M1 and  $H = 130.3$  AU for models M2 and M3. The thickness of the disks is chosen so that it is resolved with 5 cells (at the maximum resolution of the adaptive grid) in all simulations. We assume a power law for the disk column density,  $\Sigma = 3.47 \times 10^{23} R^{-3/2} \text{ g cm}^{-2}$ , where  $R$ , given in cm, is the cylindrical radius measured outwards from the disk axis (Johnstone et al. 1998), and a Gaussian vertical density distribution, as expected from an isothermal standard disk model (Pringle 1981; Hartmann 1998; Frank, King, & Raine 1992). We should note that we had to use a constant thickness due to the fact that, with the adopted numerical resolution, a more realistic disk model would not be feasible. For instance, a disk with a scale height that follows the ratio  $H/R \sim 0.1$  (Papaloizou & Terquem 1999), provides a thickness of the order of 0.001 AU and 10 AU for the internal (0.01 AU) and external (100 AU) disk radius, respectively. Both of them are smaller than the cell length of our finest grid resolution, which is  $\simeq 26$  AU. Of course, we could improve the resolution to treat the disk properly. However, we found it difficult numerically. In fact, models M2 and M3, which have cells of 6 AU, converge very slowly in time. Moreover, in order to keep the morphological features inside the computational box (such as the interaction between the photoevaporated flows and the wind), we should have thousands of grid cells (in  $x$ ,  $y$  and  $z$ ) which would result in an inordinately long computational time.

The dynamics of the disk are not taken into account as we do not include in our simulations the gravitational potential of the low mass, central star. With the chosen surface densities we obtain theoretical disk masses of  $0.097 M_{\odot}$  for the disk with a radius of 130 AU,  $0.087 M_{\odot}$  for the 104 AU disk radius, and  $0.05 M_{\odot}$  for the 30 AU disk radius (see Table 1).

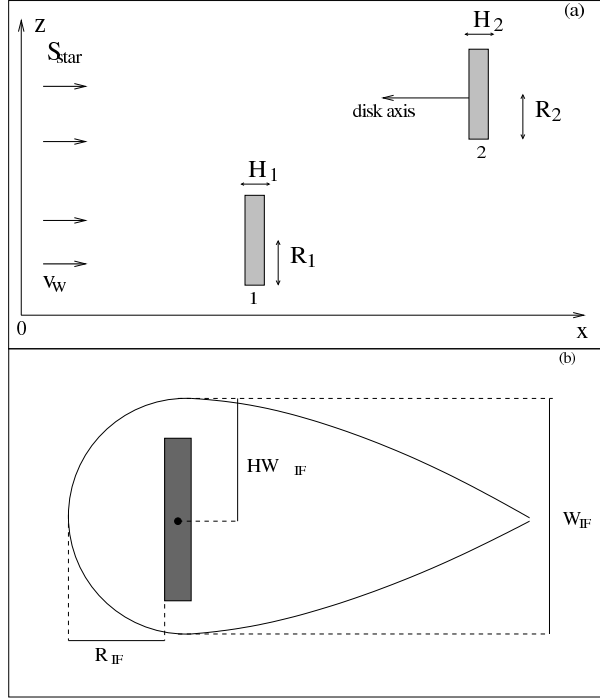


Fig. 1. (a) Schematic view of the initial setup of the simulations. (b) Definitions of the IF radius ( $R_{\text{IF}}$ ), IF width ( $W_{\text{IF}}$ ) and IF half width ( $HW_{\text{IF}}$ ).

The initial setup of the simulations is shown in Figure 1a, in which we have two disks with radius  $R_1$  and  $R_2$  and thicknesses  $H_1 = H_2 = H$ . The thickness of the disks as well as the disk axes lies in the  $x$ -direction. The stellar UV source is located outside the computational domain, along the  $x$ -direction. Furthermore, the disk axes of the two disks are parallel to the impinging ionizing/dissociating radiative field. The distance between the center of the disks/proplyds is of 2 000 AU for models M0 and M1 and  $\simeq 200$  AU for models M2 and M3 (see Table 1). In all the models, the region outside the disks is filled with a uniform, ionized medium of density  $500 \text{ cm}^{-3}$ . A wind with a velocity  $v_w = 50 \text{ km s}^{-1}$  and a density  $n_w = 500 \text{ cm}^{-3}$  is injected into the computational domain every timestep in a direction parallel to the impinging ionizing/dissociating radiative field (positive  $x$ -direction). Although a  $50 \text{ km s}^{-1}$  wind velocity does not represent the  $\theta^1$  Ori C wind, which has estimates ranging from  $500 \text{ km s}^{-1}$  to  $1650 \text{ km s}^{-1}$  (Bally et al. 1998), we would like to stress that, on the other hand, the ram pressure of our modeled wind,  $\rho v_w^2 \simeq 2,7 \times 10^{-8} \text{ dyn cm}^{-2}$  is comparable to that expected for the wind from  $\theta^1$  Ori C at the position of LV1, which is  $\approx 2.2 \times 10^{-9} \text{ dyn cm}^{-2}$ . The regions where the ram pressure of the O star wind

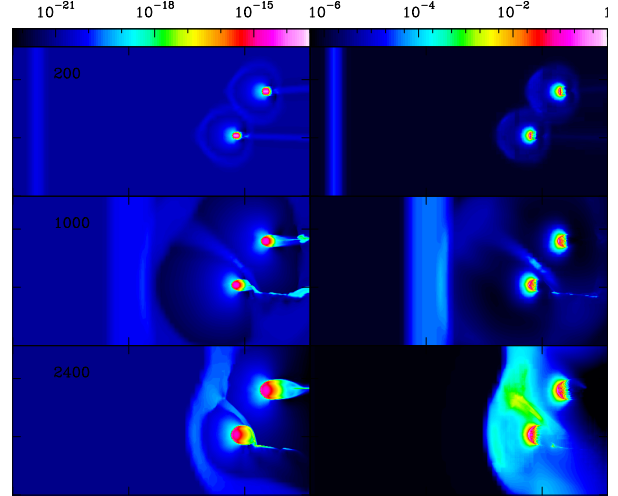


Fig. 2. Temporal evolution ( $t = 200$  yr, top;  $t = 1000$  yr, middle;  $t = 2400$  yr, bottom) of density (left) and  $H\alpha$  emission maps (right) for model M0, with no FUV radiation (see Table 1 for details). The density stratifications (in the plane containing the axes of the two disks) are shown with a logarithmic scale, which is given (in  $\text{g cm}^{-3}$ ) by the top left bar. The intensity maps (computed by integrating the  $H\alpha$  emission coefficient along lines of sight assuming that the disks axes coincide with the plane of the sky), are shown on a logarithmic scale. The scale is normalized by the maximum  $H\alpha$  intensity. The displayed domain has a physical size of  $(13.3 \times 6.6) \times 10^3$  AU.

matches the ram pressure of the photo-evaporated flow define the wind (or bow) shock position, which is generally associated with the  $[\text{O III}] + H\alpha$  arc observed in many Orion proplyds (Bally et al. 1998, see their Figure 3). Since in our simulations the ram pressure is greater than the estimated value for the  $\theta^1$  Ori C wind, the shock equilibrium position will be closer to the star than the observed structure.

Also, in Figure 1 (Figure 1b) we show some proplyd length definitions used throughout the text. Table 1 summarizes the parameters of the computed models.

### 3. RESULTS

Figure 2 shows the evolution of the density stratification (left) and  $H\alpha$  emission (right) for model M0 (which has no FUV radiation flux, see Table 1) in the  $xz$ -plane. The three snapshots correspond to different evolutionary stages: 200 yr (top), 1 000 yr (center) and 2 400 yr (bottom).

There are three structures surrounding the disks: a wind shock, which travels along the ambient medium until it encounters the photo-evaporated flows, the interproplyd shell, which is a result of the interaction between the two photo-evaporated flows,

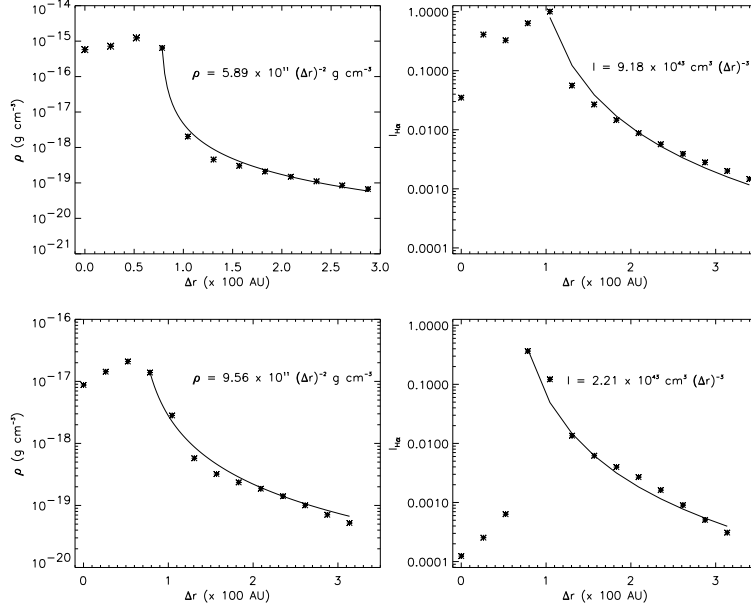


Fig. 3. Density (left) and normalized H $\alpha$  intensity (right) profiles as a function of the distance for disk models with distinct surface density laws. From top to bottom,  $\Sigma = 3.47 \times 10^{23} R^{-3/2} \text{ g cm}^{-2}$  (from model M0) and  $\Sigma = 4.63 \times 10^{22} R^{-3/2} \text{ g cm}^{-2}$ . The points were taken along the symmetry axis of proplyd 1 (see Figure 1) and are separated by one cell unit,  $\Delta x$ . Distances were measured from the disk center. The solid curves represent the best fit to the data of the ionized flow.

and an elongated structure that appears behind the disks, which is related to the tails. However, since we have not treated the diffuse radiation field, these elongated structures have densities that are too low when compared to the real proplyd tails in Orion.

Initially (at  $t = 200$  yr, top panels of Figure 2), the EUV field begins to photo-evaporate the two disks. The photo-evaporated flows start to interact with each other, and the shock front due to the wind just starts to travel from the left of the computational domain towards the binary system.

At later evolutionary times ( $t = 1000$  yr, central panels), the wind starts to interact with the photo-evaporated flows from the proplyds. The interaction between the two photo-evaporated flows (see the H $\alpha$  map in Figure 2; center-right panel) starts to produce the so-called “interproplyd shell”.

At later stages ( $t = 2400$  yr, bottom panel) the bow shock surrounding the two proplyds becomes approximately stationary, adopting an asymmetric configuration. Approximately stationary, in this case, refers to the fact that until this time, the wind shock has travelled from the left of the computational domain towards the binary disks, and then stopped at the position shown in the bottom panel of Figure 2 due to the ram pressure balance between the impinging wind and the photo-evaporated flows.

From this point to the end of the run (at  $\approx 5000$  yr), this interaction region does not change in a significant manner: both the position of the bow shock and its morphological features are approximately constant in time.

Another interesting feature is the disruption of the tail of proplyd 1 due to the interaction with the photo-evaporated wind from proplyd 2. We should note that, due to the absence of diffuse radiation field in our simulations, the tail structures that we obtain do not represent the real configuration that occurs in the Orion proplyds. The interproplyd shell glows in H $\alpha$ , but the H $\alpha$  intensity of the ionization front (hereafter, IF) of each proplyd (H $\alpha_p$ ) is greater than the intensity of the shell (H $\alpha_{\text{IPS}}$ ). In particular, if we choose the maximum emission in the corresponding regions, we find that the proplyd emission is greater than the interproplyd shell emission by factors of H $\alpha_p$ /H $\alpha_{\text{IPS}} \approx 250$ .

The base of the photo-evaporated flow from each of the proplyds is not affected by the presence of the other proplyd. Each photoevaporated flow shows a behavior compatible with a photoionized system or EUV-dominated flow (Johnstone et al. 1998) for models where the  $S_{\text{FUV}}$  photon flux is zero. In order to show this, in Figure 3, we plot on the left and on the right panels density and normalized H $\alpha$

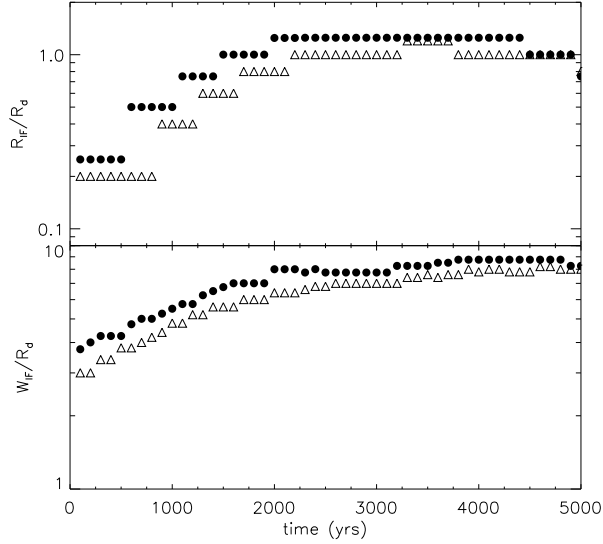


Fig. 4. Top panel: evolution of the distance of the H $\alpha$  emission peak to the original disk surface ( $R_{\text{IF}}$ , see Figure 1b) normalized by the disk radius ( $R_d$ ) for model M0. Filled circles represent the data for proplyd 1 and opened triangles are data from proplyd 2 (see Figure 1a for the initial setup of the models). Bottom panel: IF width ( $W_{\text{IF}}$ , see Figure 1b) divided by the disk radius ( $R_d$ ) for proplyds 1 (filled circles) and 2 (opened triangles). See text for details.

intensity profiles, respectively, measured for proplyd 1 (see Figure 1a) as a function of distance from the disk center, where the central star, if present in our simulations, would be located. The points were obtained along the proplyd symmetry axis ( $x$ -axis in our simulations). Fitting procedures take into account only those points ahead of the IF in the ionized flow, in order to show the behavior of the density and H $\alpha$  intensity profiles. Top panels show the results for model M0 (see table 1) at  $t = 2400$  yrs and bottom panels show the density and H $\alpha$  intensity profiles for an identical simulation except by the surface density profile of the disk given in this case by  $\Sigma = 4.63 \times 10^{22} R^{-3/2}$ . We note that the density of the ionized gas falls off as  $(\Delta r)^{-2}$  for both models. The normalized H $\alpha$  intensity falls off approximately as  $(\Delta r)^{-3}$ . We can say that the profiles are identical, independent of the disk masses which are equal to  $0.087 M_{\odot}$  for disk 1 of model M0 and  $0.01 M_{\odot}$  for the disk with the  $\Sigma$  profile shown above.

From Figure 2, it is clear that the radius of curvature of the IF of each proplyd grows with time. However, the radius of the IF stops growing as the system evolves, as can be checked in Figure 4. In the top panel of this figure, we plot the distance of the peak

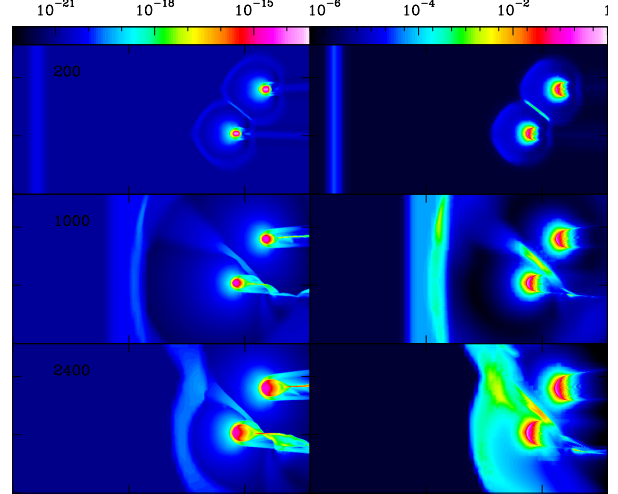


Fig. 5. Temporal evolution ( $t = 200$  yr, top;  $t = 1000$  yr, middle;  $t = 2400$  yr, bottom) of density (left) and H $\alpha$  emission maps (right) for model M1, with both EUV and FUV radiation (see Table 1 for details). The density stratifications are shown with a logarithmic scale, which is given (in  $\text{g cm}^{-3}$ ) by the top left bar. The intensity maps are shown with a logarithmic scale normalized by the intensity of the peak. The displayed domain has the same physical size as in Figure 2.

of the H $\alpha$  emission to the initial disk surface, called here IF radius ( $R_{\text{IF}}$ , defined in Figure 1b) as a function of time for both proplyds. In the bottom panel, we show the evolution of the IF width ( $W_{\text{IF}}$ , also defined in Figure 1b). The filled circles represent the measurements for proplyd 1 and the open triangles are for proplyd 2 (see Figure 1a). Both  $R_{\text{IF}}$  and  $W_{\text{IF}}$  are divided by the initial disk radius of each proplyd, which are equal to 104 AU for proplyd 1 and 130 AU for proplyd 2 (see Table 1). It can be noted that the radius of the IF grows with time until it reaches approximately the value of the disk radius (the jump in the values is equivalent to one cell length). This is what is expected for EUV-dominated flows, as shown by Johnstone et al. (1998).

Figure 5 shows the evolution of the midplane density (left) and H $\alpha$  emission (right) for model M1 (see Table 1), which has both the FUV and the EUV fluxes turned on but which is otherwise similar to model M0. As in the previous figure, we show the time evolution of the system, from the beginning of the wind propagation (clearly seen on the left of the top panel) until it encounters the two photo-evaporated winds and forms a stationary bow shock.

Several differences can be seen between Figures 5 and 2. For example, the density maps in Figure 5 show an envelope of dense material, slightly detached

from the disk surfaces, which corresponds to the PDRs. As in model M0, model M1 develops an interproplyd shell. In this case, however, the ratio of H $\alpha$  intensities is somewhat smaller than in model M0:  $H\alpha_p/H\alpha_{IPS} \approx 80$ .

In Figure 6, we show the midplane density stratification (top-left) and the H $\alpha$  emission map (top-right) for model M2 at  $t = 200$  years. In this model, the distance between the center of the two disks is of 214 AU and the disks have radii of 30 AU. We note that such small disks must have a central star of very low mass ( $M_\star < 0.3 M_\odot$ ) in order to launch a photodissociated flow from the disk surface. This is because the gravitational radius,

$$R_g = \frac{GM_\star}{c_s^2}, \quad (2)$$

in this case, is of the order of the disk radius,  $R_g \simeq 28$  AU. This low mass value for central stars is not uncommon in the Trapezium cluster (Hillenbrand 1997). There is also evidence that LV1 is a low mass binary system (Petr 1998). Henney (2002) pointed out that the disks of LV1 should have radii smaller than 50 AU. Moreover, Johnstone et al. (1998) estimate a radius of about 27 AU for LV1 (see Table 1 in that work). Thus, we believe the model is valid since the central star is a low mass star.

Since the distance from the proplyds to the ionizing source is taken to be  $\simeq 0.1$  pc ( $2 \times 10^4$  AU), this model corresponds to a FUV dominated model of Johnstone et al. (1998) and presents two thick PDRs. The IF for each proplyd is not hemispherical, as can be noted by the measures of the IF radius and half width (Figure 1a) which are equal, respectively, to 85 AU and 137 AU for proplyd 1. The IF radius of proplyd 2 has the same value of 85 AU. Since both disks are identical and their distances to the ionization source are approximately the same (proplyd 2 is at a distance 0.01% greater than the distance of proplyd 1) we can suppose that its half width is also equal to 137 AU. As the projected distance between the proplyds in the  $z$ -direction (from center to center) is equal to 133 AU, they overlap as can be seen in Figure 6. This implies that the interproplyd shell lies within the PDR, and its H $\alpha$  emission is mixed with the PDRs' H $\alpha$  emission. The H $\alpha$  emitting region coincides with the external envelope of the PDR (see the top right panel of Figure 6).

We have also simulated another close binary proplyd system (separation of 200 AU) but located at a distance of 0.01 pc (2000 AU) from the stellar source (model M3). This model is supposed to better represent the case of the LV1 proplyd. In the

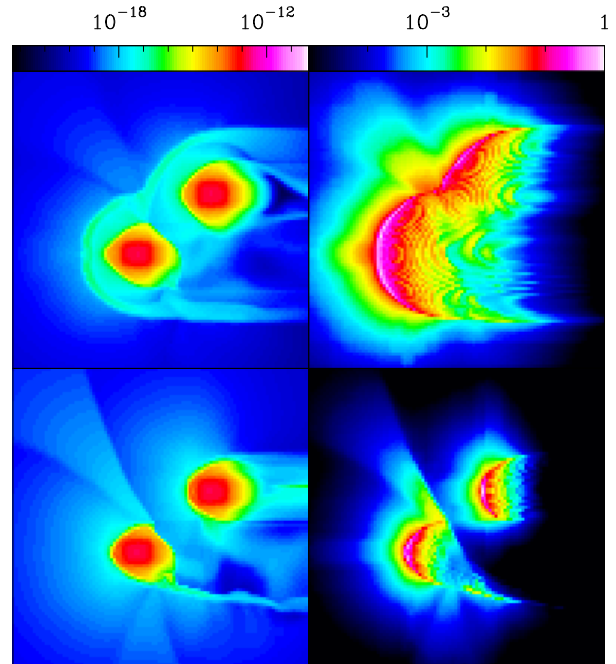


Fig. 6. A closer view of the density (left) and H $\alpha$  emission maps (right) for models M2 (top) and M3, both with EUV and FUV radiation (bottom; see Table 1) at  $t = 200$  yr. See the text for details. The density stratifications are shown with a logarithmic scale, which is given (in  $\text{g cm}^{-3}$ ) by the top left bar. The intensity maps are shown with a logarithmic scale normalized to the intensity of the maximum H $\alpha$  emission. The displayed domain has a physical size of  $(652.4 \times 652.4)$  AU.

bottom part of Figure 6 we show the midplane density stratification (bottom-left) and the H $\alpha$  emission map (bottom-right) for model M3 at  $t = 200$  years. In this case, the thickness of both PDRs is  $\simeq 13$  AU. As the PDR regions in this case are thinner, the H $\alpha$  emission map is more complex (bottom-right panel), showing that the two IFs are separated by a filamentary structure, which is due to the interproplyd shell.

We have calculated the mass loss rate of our models. Taking disk 1 of model M1, we construct Figure 7, where we plot the disk mass (top panel) and the disk mass loss rate (bottom panel). The mass loss rate for this model varies around a mean value equal to approximately  $(2.4 \pm 1.4) \times 10^{-6} M_\odot \text{ yr}^{-1}$ . This is an order of magnitude higher than the value estimated for LV1 by Johnstone et al. (1998) which is equal to  $2.24 \times 10^{-7} M_\odot \text{ yr}^{-1}$ . However, using their analytical formulae we obtain for model M1 that  $\dot{M} = 2 \times 10^{-7} \epsilon M_\odot \text{ yr}^{-1}$ , where  $\epsilon = N_{D,21} \cdot v_{0,3}$ ,  $N_{D,21}$  is the PDR column density in units of  $10^{21} \text{ cm}^{-2}$  and  $v_{0,3}$  is the PDR flow velocity in units of

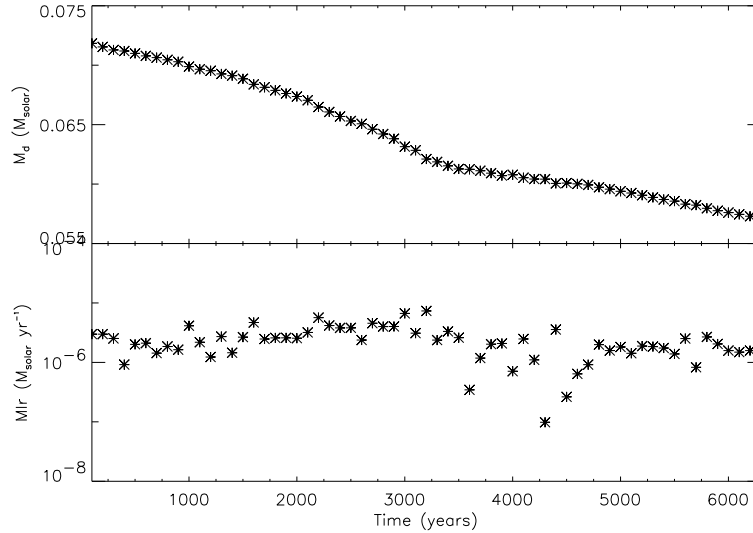


Fig. 7. Top: Disk mass for proplyd 1 of model M1. Bottom: Mass loss rate for disk 1 of the same model. See text for discussions.

3 km s<sup>-1</sup>. In measuring the column density, we obtain a mean value of  $\sim 4 \times 10^{21}$  cm<sup>-2</sup> which applied to the mass loss rate expression gives a value equal to  $9 \times 10^{-7} M_{\odot}$  yr<sup>-1</sup> which is similar to the mean value shown above. For the other models, we obtain approximately the same mass loss rate.

The disk mass obtained in Figure 7 is about 3 times higher than the disk mass derived for LV1 by Johnstone et al. (1998) (but lower than the value estimated analytically in § 2, equal to  $0.087 M_{\odot}$ ). The radii of the disks in this model are greater than the values inferred by Henney (2002) for LV1's disks which are less than 50 AU, more compatible with the disks of model M3. For them, we obtain a disk mass of approximately  $0.04 M_{\odot}$ , closer to Johnstone et al's value. This difference in the masses can be due to the surface density law we are using.

#### 4. DISCUSSION AND CONCLUSIONS

We have presented first results from three-dimensional numerical simulations of proplyds being photo-evaporated by both a FUV and an EUV radiation field. We study the specific problem of a binary proplyd system. Calculations of the H $\alpha$  emission confirm the appearance of a region of enhanced emission between the proplyd pair, the so-called interproplyd region in three out of our four simulated models. We find that the relative H $\alpha$  emission of this region is increased (by a factor of  $\sim 3$ ) if we take into account the FUV radiation for the models with greater proplyd separation (models M0 and M1). We also find that the standoff shock caused

by the interaction of the photo-evaporated flows and the stellar wind (which has been simulated here as an environmental wind of 50 km s<sup>-1</sup> and a particle density of 500 cm<sup>-3</sup>) is distorted by the presence of two disks, in agreement with the HST image of LV1 (Bally et al. 1998; Graham et al. 2002).

We have run two variations of model M1 with different limiting temperatures for the PDR ( $T_2 = 800$  K and  $T_2 = 400$  K, see equation 1). Our results show that the IF radius decreases with temperature, but the ratio of the IF H $\alpha$  emission to the interproplyd shell H $\alpha$  emission ( $H\alpha_P/H\alpha_{IPS}$ ) increases, giving values which are too high compared with the observations. These results reinforce the previous estimates for PDR temperatures of the proplyds in Orion of  $\approx 1000$  K made by Tielens & Hollenbach (1985) and Johnstone et al. (1998).

We have also simulated a close binary proplyd system (separation of  $\simeq 200$  AU) at different distances from the ionizing source:  $2 \times 10^4$  AU, which corresponds to the FUV dominated model (model M2), and  $2 \times 10^3$  AU, the case of the EUV dominated model (model M3). In agreement with the observations of LV1, we find that the EUV dominated model presents an interproplyd shell with visible H $\alpha$  emission. This does not occur in the FUV dominated model, which only shows a strongly asymmetric ionization front. Therefore, we would not expect to see interproplyd shells in binary proplyds at distances of  $\sim 0.1$  pc from  $\theta$  Orionis.

We should highlight that our model M3, which better represents LV1, has some differences from the



actual LV1 parameters. The projected distance between the proplyds, which in the HST H $\alpha$  image (Bally et al. 1998; Graham et al. 2002) is equal to  $\sim 0''.4$  (172 AU for a 430 pc distance to Orion) in our model is equal to 214 AU. The angle  $i$  of the system to the line of sight (the angle between our  $x$ -direction and the observer) is not precisely known. Henney (2002) calculates it to be equal to  $150^\circ$ . The H $\alpha$  map of Figure 6 (right bottom panel) was obtained supposing an angle  $i = 90^\circ$ . From the HST H $\alpha$  image, the emission rate between 168-326 SE's (corresponding to our proplyd 1 - see Figure 1a) IF and the peak of the interproplyd shell is  $\sim 3.4$ . In our model M3, this value is equal to 13.4.

When compared with the FUV M2 model, we can state that the EUV M3 model enhances the H $\alpha$  emission of the interproplyd shell relative to the emission from the ionization fronts, and makes the prediction more compatible with the observed values. Improvements in the treatment of the radiation field, which should take into account the diffuse radiation, as well as in the tuning of the model parameters, might result in better predictions compared with the observations.

We acknowledge an anonymous referee for comments and suggestions. MJV would like to thank FAPESB for partial financial support (PPP project 7606/2006). AHC wish to thank the Brazilian agency CNPq for partial financial support (projects 308635/2006-0 and 471254/2008-8), and also PROPP-UESC (projects 609 and 635). AR acknowledges support from the DGAPA (Universidad Nacional Autónoma de México) grant IN108207, from the Conacyt grant 61547, and from the "Macroproyecto de Tecnologías para la Universidad de la Información y la Computación (Secretaría de Desarrollo Institucional de la Universidad Nacional Autónoma de México).

## REFERENCES

- Bally, J., Sutherland, R. S., Devine, D., & Johnstone, D. 1998, *AJ*, 116, 293
- Cerqueira, A. H., Cantó, J., Raga, A. C., & Vasconcelos, M. J. 2006a, *RevMexAA*, 42, 203
- Cerqueira, A. H., Velázquez, P. F., Raga, A. C., Vasconcelos, M. J., & De Colle, F. 2006b, *A&A*, 448, 231
- Frank, J., King, A., & Raine, D. 1992, *Accretion Power in Astrophysics* (3rd ed.; Cambridge: Cambridge Univ. Press), 89
- García-Arredondo, F., Henney, W. J., & Arthur, S. J. 2001, *ApJ*, 561, 830
- Graham, M. F., Meaburn, J., Garrington, S. T., O'Brien, T. J., Henney, W. J., & O'Dell, C. R. 2002, *ApJ*, 570, 222
- Hartmann, L. 1998, *Accretion Process in Star Formation* (1st ed.; Cambridge: Cambridge Univ. Press), 91
- Henney, W. J. 2002, *RevMexAA*, 38, 71
- Hillenbrand, L. A. 1997, *AJ*, 113, 1733
- Johnstone, D., Hollenbach, D., & Bally, J. 1998, *ApJ*, 499, 758
- Lefloch, B., & Lazareff, B. 1994, *A&A*, 289, 559
- Levermore, C., & Pamraning, G. 1981, *ApJ*, 248, 231
- Lim, A. J., & Mellema, G. 2003, *A&A*, 405, 189
- Mellema, G., Raga, A. C., Cantó, J., Lundqvist, P., Balick, B., Steffen, W., & Noriega-Crespo, A. 1998, *A&A*, 331, 335
- O'Dell, C. R., & Wen, Z. 1994, *ApJ*, 436, 194
- O'Dell, C. R., & Wong, K. 1996, *AJ*, 111, 846
- Papaloizou, J. C. B., & Terquem, C. 1999, *ApJ*, 521, 823
- Petr, M., Coude Du Foresto, V., Beckwith, S., Richichi, A., & McCaughrean, M. 1998, *ApJ*, 500, 825
- Pringle, J. E. 1981, *ARA&A*, 19, 137
- Raga, A. C., Navarro-González, R., & Villagrán-Muñiz, M. 2000, *RevMexAA*, 36, 67
- Raga, A. C., Noriega-Crespo, A., Cantó, J., Steffen, W., van Buren, D., Mellema, G., & Lundqvist, P. 1997, *RevMexAA*, 33, 73
- Richling, S., & Yorke, H. W. 2000, *ApJ*, 539, 258
- Smith, N., Bally, J., Licht, D., & Walawender, J. 2005, *AJ*, 129, 382
- Störzer, H., & Hollenbach, D. 1999, *ApJ*, 515, 669
- Tielens, A.G.G.M., & Hollenbach, D. 1985, *ApJ*, 291, 772
- van Leer, B. 1982, ICASE Report No. 82-30

Rafael R. Amorim: Instituto Nacional de Pesquisas Espaciais/MCT, Av. dos Astronautas, 1758, CEP 12227-010, São José dos Campos, São Paulo, Brazil (rafael\_rei\_amorin@yahoo.com.br).

Adriano H. Cerqueira and Maria J. Vasconcelos: Laboratório de Astrofísica Teórica e Observacional, DCET-UESC, Rodovia Ilhéus-Itabuna, km. 16 Ilhéus, Bahia, CEP 45662-000, Brazil (hoth, mjvasc@uesc.br).

Alejandro C. Raga: Instituto de Ciencias Nucleares, Universidad Nacional Autónoma de México, Apdo. Postal 70-543, 04510, México, D. F., Mexico (raga@nucleares.unam.mx).